

Electron channeling studies of local surface deformation in HSLA steel

M. KACZOROWSKI¹⁾ and WILLIAM W. GERBERICH.

Department of Chemical Engineering and Materials Science, University of Minnesota, Minneapolis, Minnesota, U.S.A.

Abstract

The deformation process in high strength low-alloy (HSLA) steel has been investigated using transmission and scanning electron microscopy. Electron channeling contrast and selected area channeling pattern (SACP) techniques reveal microscopic orientation changes developing during deformation by tension. Theoretical modeling involves an accounting procedure based on dislocations emanated at grain boundary sources. This has shown that a length scale (subcell diameter) might be utilized to predict strain-hardening behavior with a dislocation source length coefficient of ~ 2.2 and Taylor work hardening coefficient, $\alpha = 0.44$.

Riassunto

Studi mediante electron channeling di deformazione locale superficiale in acciaio HSLA

Il processo di deformazione in acciaio bassoalegato ad alta resistenza (HSLA) è stato investigato mediante l'impiego del microscopio elettronico a trasmissione e a scansione. Le tecniche di contrasto con electron channeling e di selected area channeling pattern (SACP) rivelano variazioni microscopiche di orientamento durante la deformazione per trazione. Il modello teorico comprende una procedura interpretativa basata sull'analisi delle dislocazioni create dalle sorgenti a bordo grano. Questo ha dimostrato che una scala di lunghezza (diametro di subcella) può essere utilizzata per prevedere il comportamento all'incrudimento con un coefficiente di lunghezza di sorgente di dislocazione pari a $\sim 2,2$ e con un coefficiente di incrudimento di Taylor pari a $\sim 0,44$.

Introduction

Deformation in engineering materials is most commonly described by elongation of a tensile bar. This value is very useful in design problems since it characterizes the average properties of a given polycrystalline material. This average value reflects the fact that most materials used in practice consist of many grains of different orientation with respect to the direction of loading. From the other point of view, it is well known that with increasing load to failure, a crack does not initiate from a random site but from one of several preferred nucleation sites. There are many factors making some sites more favorable for crack nucleation than others. In the case of a smooth and microstructurally uniform sample, i.e. without relatively large inclusions or precipitates or surface discontinuities, the crack will most probably nucleate at the free surface in regions of highly localized plastic flow. In polycrystalline materials it will appear in those grains whose glide systems are conveniently oriented with respect to the direction of loading. The study of the stress state for initiation of local cracking is of considerable interest for the case of textured materials. This is due to the fact that such preferred orientation might be beneficial or detrimental to crack initiation. One of the best methods for such studies seems to be the electron channeling pattern (ECP) technique, discovered by Coates in 1967^[1]. The advantages of this method are that it allows information about local deformation in areas less than $5 \mu\text{m}$ ^[2,3] and also about crystallographic orientation or the change of orientation during deformation. All of these together with traditional scanning electron microscopy (SEM)

observations give us a nearly complete local deformation history indispensable to the analysis of the crack-initiation process. In the present study, we apply this technique to the step-wise local deformation of a polycrystalline steel. First, it is useful to briefly describe some general concepts associated with electron channelling.

Theoretical background

While the detailed theory on the mechanism of ECP formation is given elsewhere^[2-7], it is useful to introduce the reader to the principal concept. What is electron channeling? In a few words, an ECP represents the variation of signal intensity resulting from changes in the angle between the incident electron beam and the crystal lattice of the specimen. This pattern, because of its geometric similarity, is sometimes called a pseudo-Kikuchi pattern^[8]. It is generated when the electron travelling in the specimen interacts with the periodic potential field. In terms of electromagnetic theory, the electron flux moving through the crystal lattice can be represented as a number of Bloch waves of the same periodicity as the lattice. These Bloch waves propagate through the crystalline body from the surface of incidence into the center with their wave front parallel to the surface normal. In the simplest case, the current travelling in the specimen is a macroscopic measure of the square of the amplitude of the Bloch waves at any point and can be resolved into just two of them. The first, Type I wave has its intensity maximum on the lines of atom centers, while the other Type II provides a maximum lying exactly between the rows of atoms (Fig. 1). Since the higher probability of the electrons in the Type I wave are to be found in close proximity to the nuclei,

1) M. Kaczorowski is on leave of absence from the Institute of Plastic Forming, Casting and Welding, Technical University of Warsaw, Poland.

this wave will be more strongly backscattered than electrons in the Type II wave. Because the ratio of Bloch wave II to I depends on the angle between the incident beam and lattice, the intensity of backscattered electrons will change as an electron beam is swept over the specimen. When the angle of incidence θ (Fig. 2) is such that the Bragg condition for the interplanar spacing, d , is satisfied, i.e.,

$$\lambda = 2 d \sin \theta$$

with λ the electron wavelength, the intensity of both Bloch waves are exactly the same. However, for an incident angle $\theta < \theta_B$, where θ_B is the Bragg angle, the intensity of wave I is greater than that of wave II and the total backscattered intensity will increase. For $\theta > \theta_B$ the intensity of wave I is less than that of wave II and fewer electrons will be backscattered.

Fig. 2 shows the situation occurring in an SEM where an electron beam is scanning over a flat surface of a crystal. As the beam is moving, the angle between it and the lattice planes changes which varies the intensity of the backscattered signal. For example at points A and B, $\theta = \theta_B$, so between them, where $\theta < \theta_B$, enhanced backscattering will occur while outside these positions, where $\theta > \theta_B$, a decreased intensity will occur with respect to the level at points A and B. These changes in the intensity of backscattered signal as a function of the position are shown below

Fig. 1. Sketch illustrating the position of Bloch waves 1 and 2 relative to lattice planes.

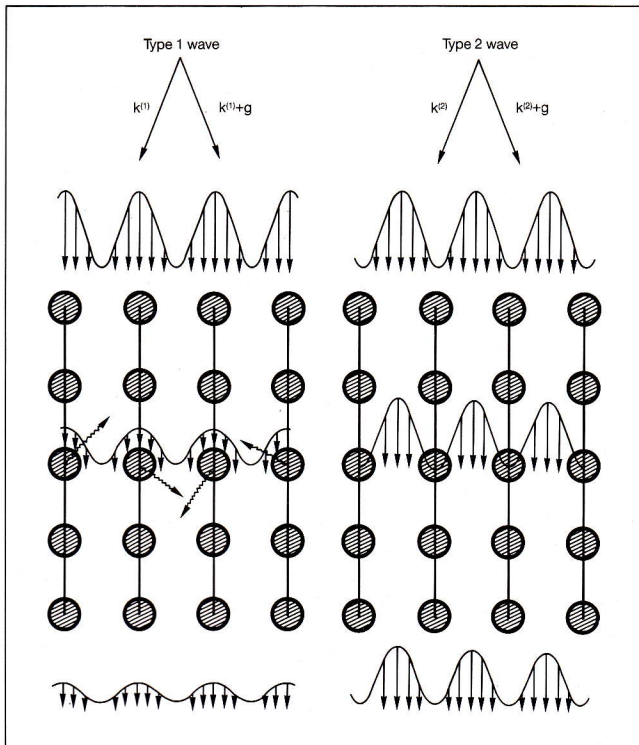
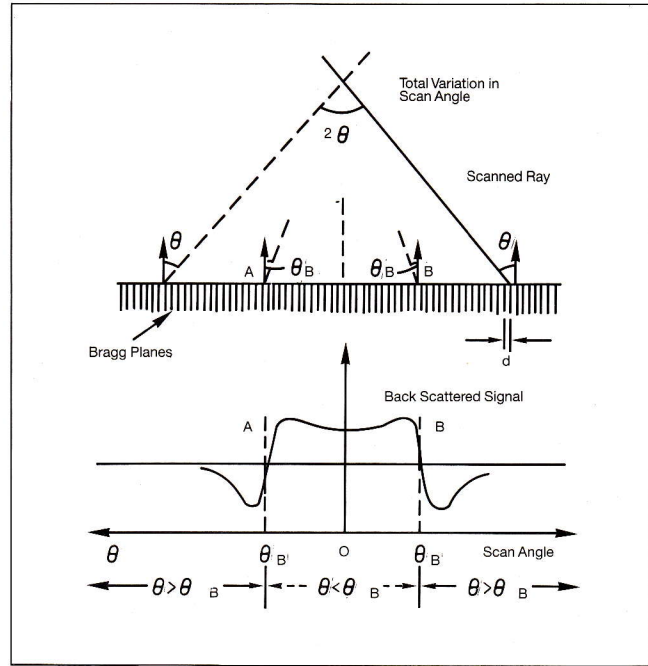


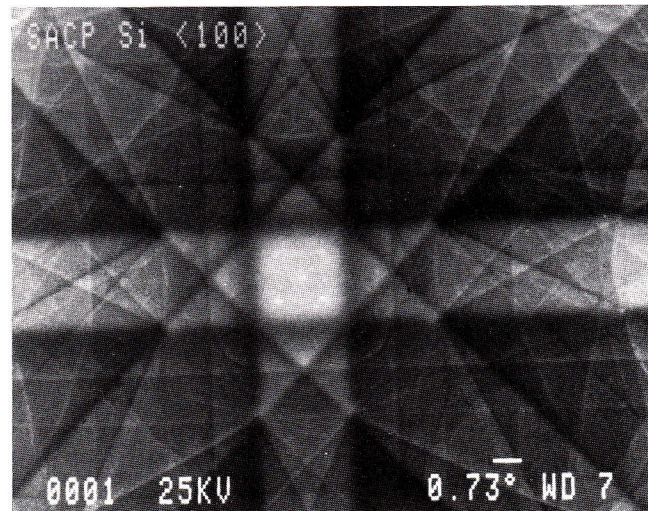
Fig. 2. Changes in the geometry of an incident beam during scanning. During any one line scan the incidence angle θ varies from being greater than θ_B to being smaller than θ_B . At two symmetric positions A and B, $\theta = \theta_B$. This variation gives the changes in backscattering signal intensity shown [7].



(Fig. 2). In the case of a two-dimensional raster with rocking, basically a cone of revolution is swept out. With this type of scan, other sets of lattice planes will contribute to the contrast with the final signal plot being an ECP. One typical example is shown in Fig. 3. It consists of many bands of different orientation and width which are strictly correlated with the geometry of the crystal lattice transformed into reciprocal space.

Of the main uses of the ECP technique, one which is analogous to x-ray line broadening is used to study the deformation process. This technique is reviewed and

Fig. 3. SACP from an $\langle 001 \rangle$ oriented silicon sample.



discussed in a number of publications which have appeared in the last ten years^[8-15]. It is the principal aspect of electron channeling which has been used in this study where localized deformation of HSLA steel is investigated.

Experimental procedure

The experiment has been performed on high strength low alloy steel (HSLA) with a composition of 0.070 C, 0.51 Mn, 0.03 Si, 0.01 Al and 0.014 Nb in weight percent. The materials were annealed to an average grain size of about 120 μm and a yield strength of 220 MPa. The specimens were miniature tensile bars with the gage diameter and length of 3 mm and 1.5 mm, respectively. To fix one position of the sample, which was repetitively introduced into the SEM, a part of the thread surfaces were removed by grinding. Then, the central piece of the specimen was polished electrochemically, first to remove the deformed layer and, secondly, to provide a clean and smooth surface. Simultaneously, the grain boundary and pearlite colonies were made visible. Before testing, the samples were observed in the SEM and a minimum of 8 grains, placed in the middle part of the gage section, were chosen. After the first set of micrographs were taken, the specimen was deformed step-wise in an MTS servohydraulic test machine, Model 810, to a given average strain level of $\epsilon \sim 0.5, 1.75, 2.5, 5, 7.5, 10$ and 15%. The actual deformation was evaluated by measuring the overall gage length in the loading direction. After each step of deformation, the specimen was observed using both secondary and backscattered electrons to investigate topographical changes and developing slip bands. Electron channeling was used either to observe grains under channeling contrast^[16] and/or to provide their SACP's. The first of these allows an evaluation of the orientation changes inside a given grain, while the second one allows SACP line degradation to be followed as an indicator of the deformation level. SEM observations were performed on a JEOL JSM-840 scanning electron microscope equipped with a special SACP attachment which provides a small spot size of the rocking beam, $d = 10 \mu\text{m}$. To obtain some information on the density and distribution of dislocations, a TEM investigation has also been performed. Thin foils were sliced from the tension specimen at a distance approximately 4 mm from the fracture surface and then electropolished using the one jet method. These samples were then observed in a JEOL-100CX transmission electron microscope operating at an accelerating voltage of 100 kV.

Results

The sequence of micrographs shown in Figs. 4 a-f

represents the change of the substructure in one of the grains as the sample is deformed by tension to different deformation levels. The local strain measured as an increase of the distance between two characteristic points on the picture has reached $\epsilon \sim 0.25$ in Figure 4f. There are two characteristic features developing in these micrographs. One of them is a set of lines representing slip planes which intersect the free surface of the grain. The next are specific areas of channeling contrast being visible because of the orientation changes inside the grains. As could be anticipated, the number of slip lines increase with deformation. Near the beginning, Fig. 4b, only one major slip system is operating at the surface of this grain. An increase of strain causes the next slip system to start, (Fig. 4c). These lines become more pronounced with deformation, i.e. compare the central part of Figs. 4c and 4f. Simultaneously, the number of places where additional slip systems start to appear is also increasing. This is probably because the strain hardening in one area forces the other systems to operate which originally had an orientation inconvenient for slip. The channeling contrast makes visible how the deformation process changes the orientation of some regions. The specific contour development has been discussed in detail by Gerberich *et al.*^[17] in which they suggest that circular or elliptical patterns may be precursors to sites where microcracks initiate. Corresponding to each stage of deformation in Fig. 4, selected area channeling patterns taken from the central part of the grain are shown in Figs. 5 a-f. The first gives the SACP from the grain without deformation. The characteristic feature of this micrograph is a number of parallel lines forming band whose intersection gives a pole. From comparison of this SACP with a part of the ECP map for the BCC system in Figs. 6 a,b^[18], it follows that the two poles observed in Fig. 5a are [113] and [135]. The sketch of the main bands visible in Fig. 5, indexed according to the ECP map, is shown in Fig. 7. The orientation of the grain evaluated on the same basis is in the proximity of a [359] pole. This orientation however is not constant but changes with an increase of deformation. It can be easily observed by following the [113] pole position. This pole shifts from the lower right corner to the left as indicated by the angular shift, $\Delta\alpha$, in Fig. 8. Simultaneously, a degradation of SACP-lines is observed. As it is well known, the degradation of ECP's proceeds by distortion of the crystal perfection as caused by any kind of defect. In the present case, the most important defects are dislocations whose density are a function of deformation. Their appearance involves distortion of lattice planes which in turn disturbs the elastic scattering process in the body. This produces an increase in the SACP-line width which becomes a measure of deformation magnitude. This has been determined using a microdensitometer trace

Fig. 4. A selected HSLA steel grain: (a) – before deformation and after deformation up to : (b) – $\epsilon = 4.3\%$, (c) – $\epsilon = 7.3\%$, (d) – $\epsilon = 10.5\%$, (e) – $\epsilon = 14\%$ and (f) – $\epsilon = 25\%$.

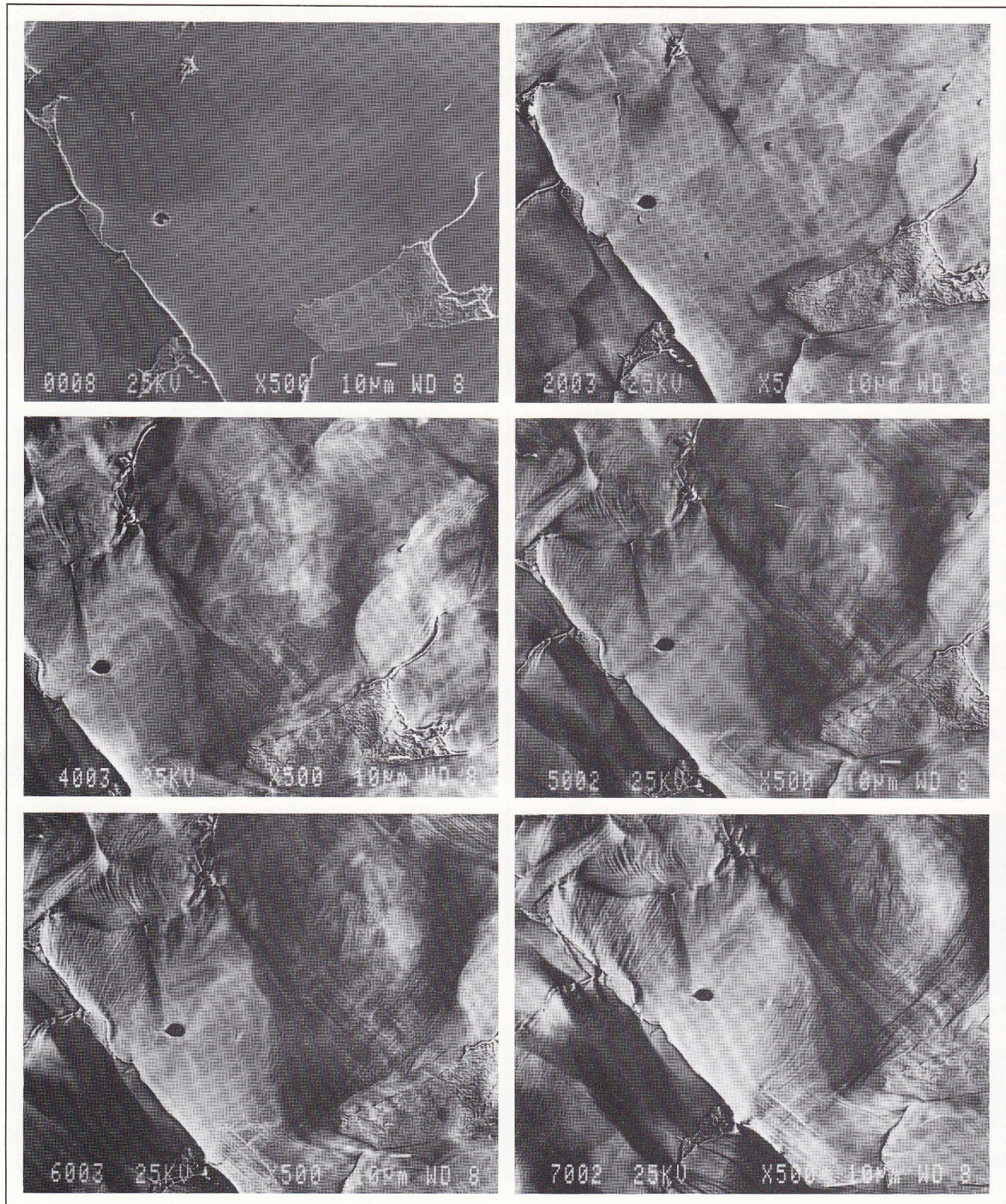


Fig. 5. SACP's from the same grain as on Fig. 4 (a) – before deformation and after deformation by tension up to: (b) – $\epsilon = 4.3\%$, (c) – $\epsilon = 7.3\%$, (d) – $\epsilon = 14\%$ and (f) – $\epsilon = 25\%$.

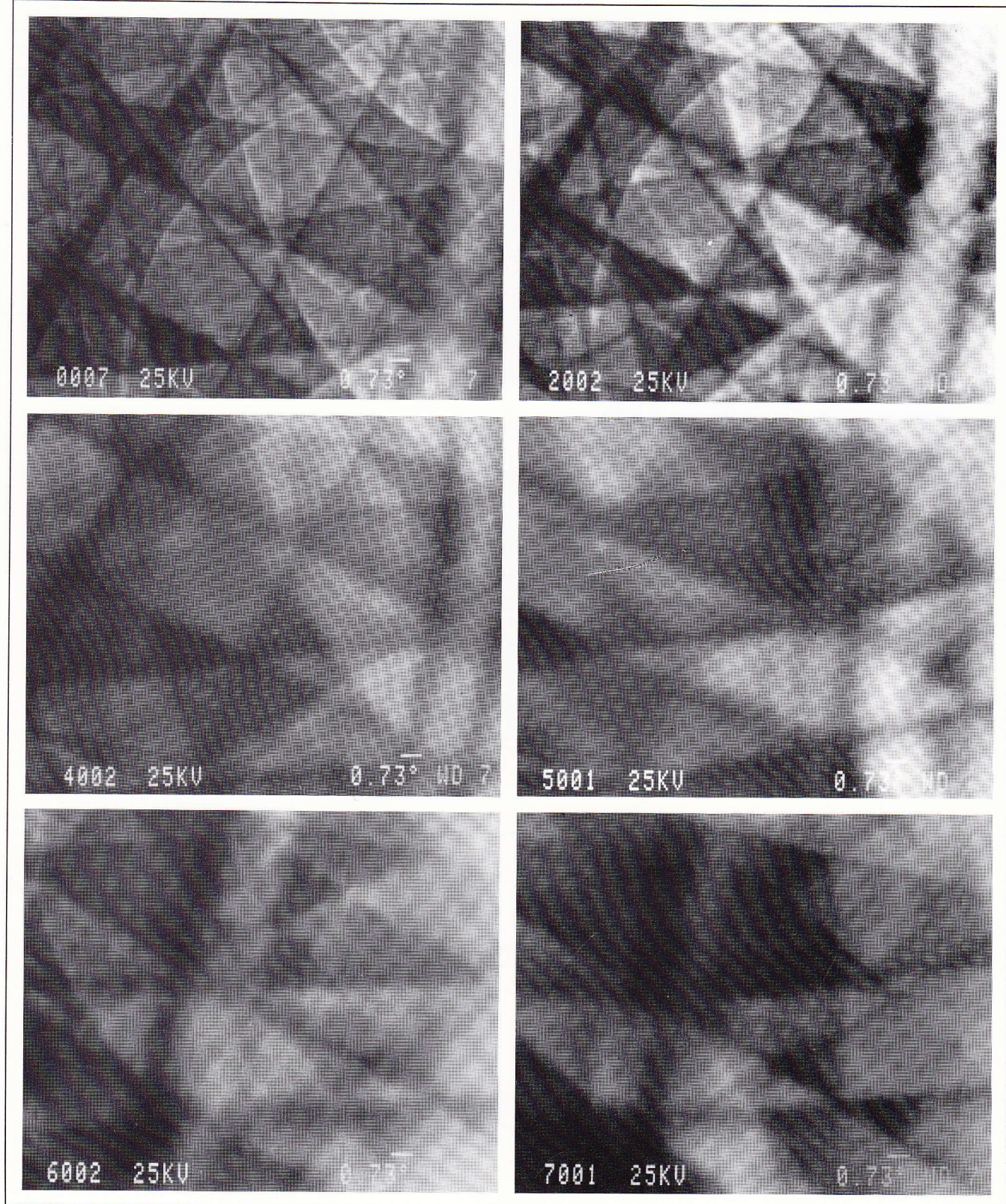


Fig. 6. (a) Part of the ECP map and (b) indexing guide for a BCC system.

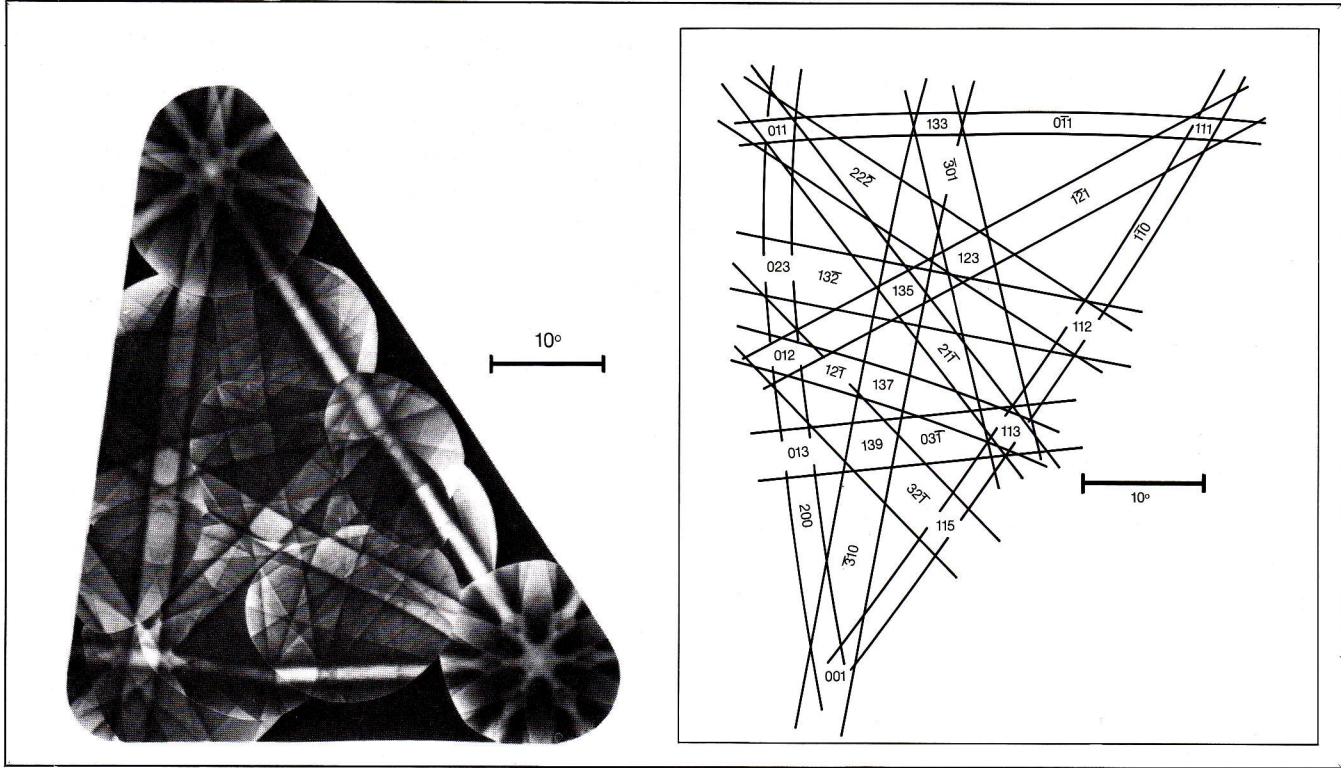


Fig. 7. Sketch of the main bands observed on an SACP indexed according to the ECP map.

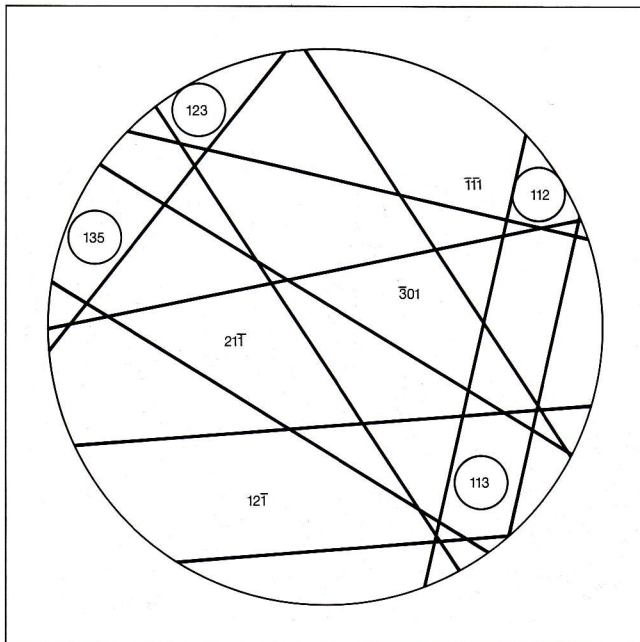
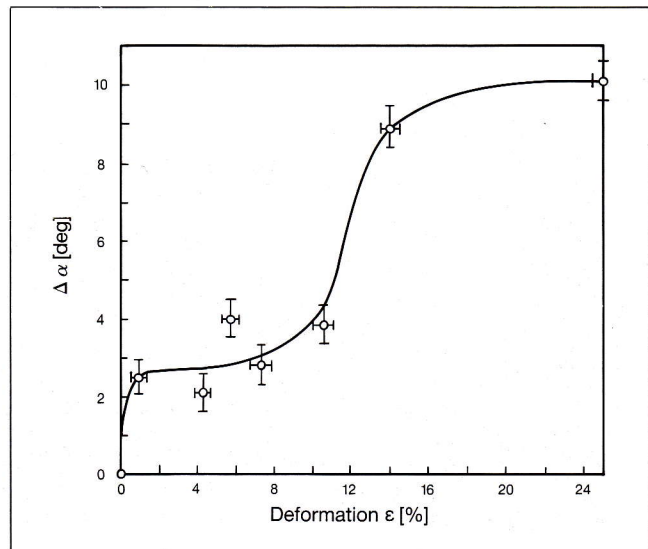


Fig. 8. The position change of the SACP center as a function of deformation level for the case shown in Fig. 5.



in the present study. These were taken across one line visible on each of the SACP's. One such microdensitometer trace is shown in Fig. 9. The next graph, Fig. 10, illustrates how the SACP line width changes with deformation. Such a calibration curve is used for evaluation of local deformation^[19,20]. The last

Fig. 9. Microdensitometer trace of the intensity distribution taken across one of SACP lines.

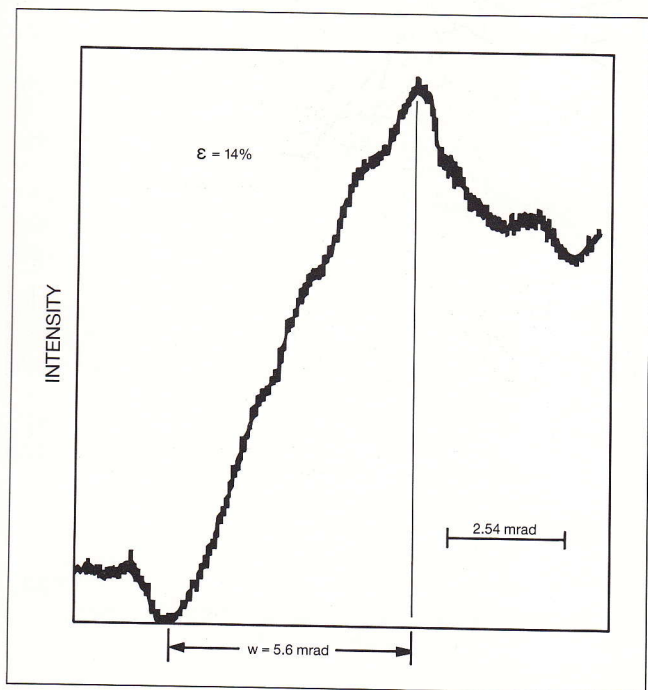
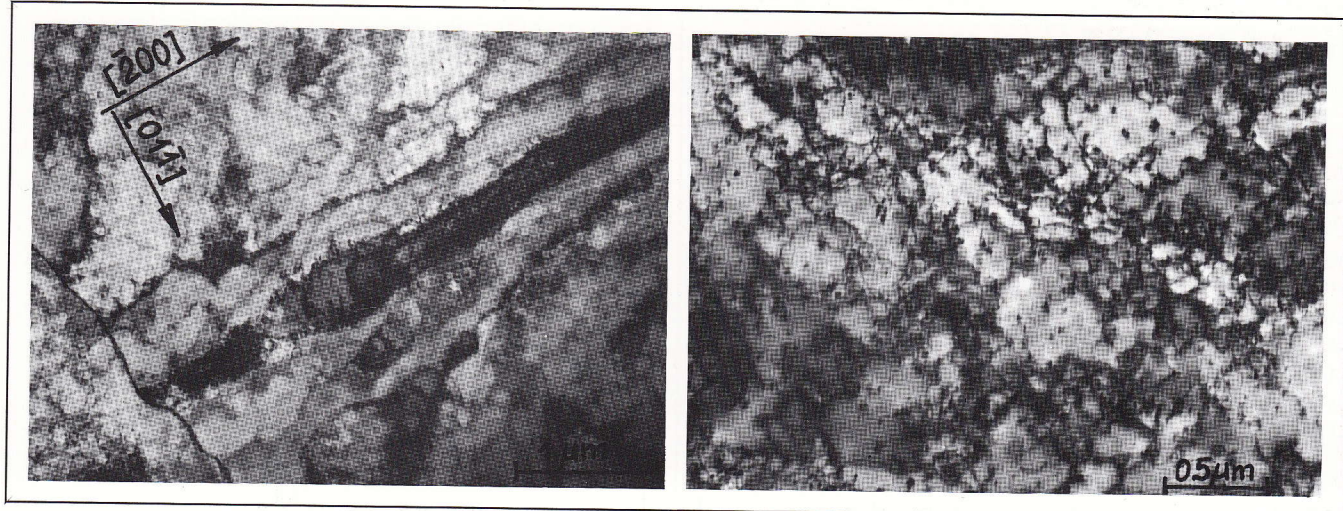


Fig. 11. Examples of the dislocation distribution in an HSLA specimen deformed by tension up to an average level, $\epsilon = 15\%$.



micrographs in Figs. 11 a,b show the distribution of dislocations in the specimen which was subjected to an average deformation of $\epsilon \sim 15\%$. As can be seen, the dislocations are not distributed randomly but tend to form subcells with rather weakly defined subcell walls. Sometimes they are elongated but on the average their diameter is about $1 \mu\text{m}$ and the dislocation density is of the order, $\rho \sim 10^{13} \text{m}^{-2}$.

Discussion

Fig. 12 is a superposition of the surface features and some crystallographic information taken from the SACP

Fig. 10. Change of the SACP-line width with deformation.

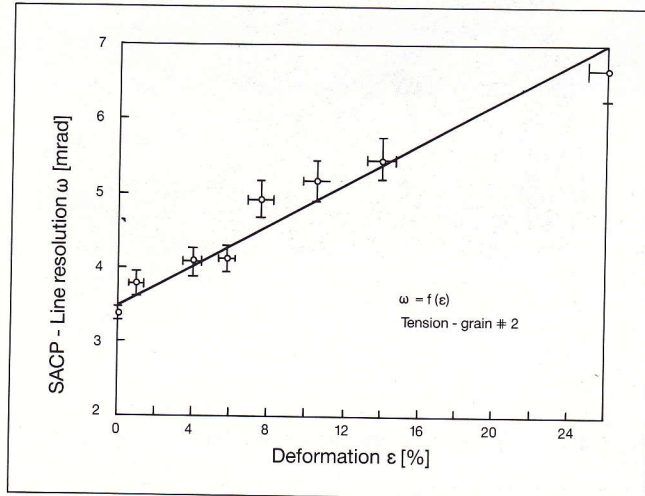
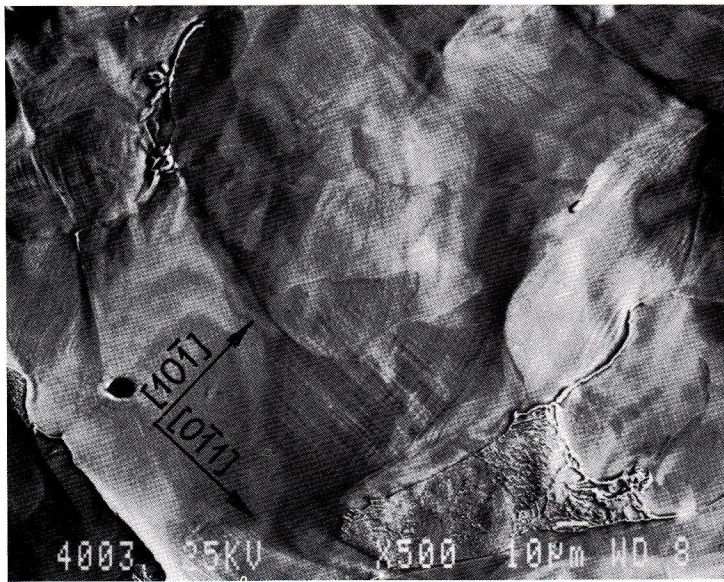


Fig. 12. Superposition of the surface features and crystallographic data taken from the SACP of the grain deformed to $\epsilon = 7.3\%$.



for the fourth stage of deformation where the strain was equal $\sim 7.3\%$. To properly orient the slip vectors, a small misorientation angle, equal to five degrees as caused by rotation of the SACP with respect to the micrograph, has been taken into account [21,22]. The set of lines show directions which were evaluated on the basis of SACP, where the bands representing planes almost perpendicular to the surface of the sample are visible. Using a stereographic projection, a trace analysis showed that $(101) [111]$ is the first slip system to start operating in the grain being considered, with the orientation $\langle 359 \rangle$. Next, the $(0\bar{1}1) [111]$ system produces dislocation motion. This is not surprising if the relative orientation of slip planes with respect to the $[359]$ pole is considered. According to the calculation the first of them form with the pole $[359]$ at an angle 63.6° and the second at 72.7° .

It is worth to note that the grain changes its orientation during the process of deformation. According to the SACP geometry we can conclude that the $[113]$ pole is moving closer to the center of the SACP. If it is assumed that this is exactly at the center, then the angles between this pole and the $(\bar{1}01)$ or $(0\bar{1}1)$ will be equal to 64.8° . It is obvious that the grain rotation depends not only on its tendency to be oriented conveniently from the point of view of its own slip systems but also on the orientation of its neighbors. Let us next use the model proposed by Gerberich *et al* [17], and their accounting procedure, to describe the length scale in dislocation patterns as produced by monotonic loading of a polycrystalline material.

According to this model, the pattern generation and dislocation spacings are dictated by the quasi-static state of equilibrium during the work hardening phase of the loading. Neglecting details, as described in the original paper, the density of geometrically necessary dislocations ρ^G can be given by

$$\rho^G = \frac{\bar{\beta} \cdot M \cdot \epsilon}{b \cdot D}; \quad 0, \bar{\beta} < \pi \quad (1)$$

where:

$\bar{\beta}$ – average source length coefficient
 M – Taylor orientation factor (here $M = 2.75$ [23])
 ϵ – tensile strain
 b – Burgers vector
 D – grain size.

In the case of a square net similar to that observed in Fig. 12, with square subcells of size, L_s , containing dislocation spaced at l_s , the dislocation density, ρ^G , will be equal to

$$\rho^G = \frac{2}{L_s l_s} \quad (2)$$

If it is assumed that the source term (Eq. 1) and stored term (Eq. 2) are equal, then the distance between dislocations in the subcell wall will be

$$l_s = \frac{2bD}{\bar{\beta} M \epsilon L_s} \quad (3)$$

For quasi-static equilibrium an increase in stress is required to continuously activate grain boundary sources. Thus if $\tau_s = \tau_{app} - \tau_o$ then

$$\tau_s = \alpha \cdot G \left[\frac{\bar{\beta} M \epsilon \cdot b}{D} \right]^{1/2} \quad (4)$$

where G is the shear modulus of elasticity. Following Gerberich *et al* [17], the cell size is thus given by

$$L_s = 4\pi\alpha \left[\frac{b \cdot D}{\bar{\beta} M \cdot \epsilon} \right]^{1/2} \quad (5)$$

and a tensile stress approaching saturation may be given by

$$\sigma = \sigma_o + M \cdot \alpha \cdot G \left[\frac{\beta \cdot M \cdot \epsilon \cdot b}{D} \right]^{1/2} \quad (6)$$

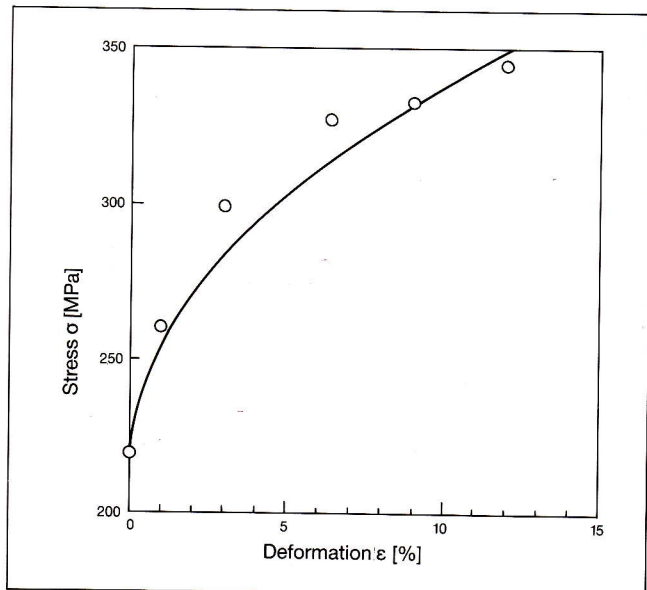
To know how σ is changing with an increase in strain, the values α , β must be evaluated. It can be accomplished using data that have been gathered in the present experiment. As was stated before, the average subcell size is about 1×10^{-6} m. This, in conjunction with known values of $M = 2.75$, $G \approx 8.3 \times 10^4$ MPa, $D = 120 \mu\text{m}$ and $\sigma_o = 220$ MPa, one may solve Eqs. (5) and (6) with one fixed point. Taking the end point for $\epsilon = 0.15$ with $\sigma = 360$ MPa, one finds that there are two equations and two unknowns, α and β . Solving these give $\alpha = 0.44$ and $\beta = 2.2$. These are both reasonable parameters and give the prediction in Fig. 13. Of course, with the initial ($\sigma_o = 220$ MPa) and final ($\sigma = 360$ MPa) points fixed, some agreement is assured. Nevertheless, the shape of the curve is reasonably well predicted.

To follow ρ^G with increasing plastic deformation, the formula given by Gerberich *et al.*^[24] may be used in conjunction with Figure 5. According to them, the dislocation density, ρ , is given by

$$\rho = \rho_o + \alpha_o(m - 0.75) \quad (7)$$

when ρ_o and α_o are constants of $2 \times 10^{12} \text{m}^{-2}$ and $10^{13} \text{m}^{-2}/\%$ strain, respectively, and m is the line

Fig. 13. Comparison of the predicted curve, Eq. 6, with experimental work-hardening data.



resolution in milliradians. If one uses the same value of $\alpha = 0.44$ as before, with the Taylor prediction, $\sigma = \sigma_o + M\alpha Gb[\rho]^{1/2}$, and the values of ρ from Figs. 5 and 10 with Eq. (7), the strain-hardening may be calculated. This overpredicts the incremental stress due to work hardening in the polycrystalline array by about 32 percent. However, this is about what would be expected since the local dislocation density in this grain was 67 percent greater and $(1.67)^{1/2}$ would be expected to give about a 30 percent increase in local hardening.

Summary

It is strongly suggested that dislocation emission starts at grain boundary sources. Depending on orientation of the slip system with respect to the direction of loading, these sources are activated step by step or simultaneously. In the first case slip bands are visible. After two or more systems are activated, these form a subcell structure with rather weakly developed subcell walls. These walls become more defined with an increase of the deformation level. The electron channeling (ECP) technique has allowed us to follow both the developing misorientation between different parts of the same crystal and a quantitative description of how the grains change their position. The data, which have been gathered using both TEM and SEM methods (including the ECP technique) make it possible to perform work hardening calculations based on a geometrically-necessary dislocation model^[17]. It was also shown that:

1. at an average strain level of $\epsilon = 15\%$ the dislocation density approached $\sim 6 \times 10^{13} \text{m}^{-2}$, but only part of the dislocation are immobilized forming loosely packed dislocation walls which are spaced at a distance of ~ 80 nm;
2. the average subcell diameter is equal approximately to $1 \mu\text{m}$; however they are weakly defined and very often elongated in one direction;
3. the subcell wave length and dislocation density are reasonably predicted with a dislocation source length coefficient of 2.2. and a Taylor work hardening coefficient of ~ 0.44 being realistic parameters;
4. multiple slip networks, being controlled by grain boundaries and the resolved shear stress, give different patterns from grain to grain and often different sets of intersecting slip inside the same grain.

Acknowledgement

The authors appreciate fruitful discussions with Dr. D.L. Davidson at the Southwest Research Institute in San Antonio. This work was supported by the Division of Materials Research of the National Science Foundation under Grant NSF/DMR-8400015.

REFERENCES

- (1) Coates, D.G. Kikuchi-like reflection patterns obtained with the SEM. *Phil. Mag.*, **16** (1967), 1179-84.
- (2) Nakagawa, S. Observation technique for micro area electron channeling patterns. *Jeol News*, **24E** (1986), 7-14.
- (3) Kaczorowski, M. Unpublished results.
- (4) Hirsch, P.B., and C.J. Humphreys. The dynamical theory of scanning electron microscope channeling patterns. In O. Johari (Ed.), *Scanning Electron Microscopy (1970)*, Proc. 3rd Annual SEM Symp., Chicago, IL, Illinois Institute of Technology Research Institute, 1979, p. 449.
- (5) Spencer, J.P., C.J. Humphreys, and P.B. Hirsch. A dynamical theory for the contrast of perfect and imperfect crystals in the scanning electrons microscope using backscattered electron. *Phil. Mag.*, **26** (1972), 193-213.
- (6) Spencer, J.P., and C.J. Humphreys. A multiple scattering transport theory for electron channeling patterns. *Phil. Mag. A*, **42** (1980), 443-451.
- (7) Joy, D.C., D.E. Newbury, and D.L. Davidson. Electron channeling patterns in scanning electron microscopy. *J. Appl. Phys.*, **53** (1982), R81-R122.
- (8) Pirouz, P., and I.M. Boswarva. Pseudo-Kikuchi pattern contrast from tiled crystals. In *Scanning Electron Microscopy: Systems and Applications* (Institute of Physics, Lond), Conf. Ser. 18, 1973, pp. 324-27.
- (9) Booker, G.R., D.C. Joy, and R. Stickler. Applications of the SEM selected area channeling pattern technique to metallurgical problems. In *Electron Microscopy and Analysis of the 25th Anniversary Meeting of E.M.A.G.* (Institute of Physics, London), Con. Serv. 10, 1971, pp. 194-197.
- (10) Schmidt, P.F., M.G. Crewe, and G. Pfefferkorn. SEM imaging of cell structures of dislocation networks in cold worked Cu single crystals. *Scanning*, **1** (1978), 174-182.
- (11) Davidson, D.L. Electron channeling, a new metallurgical tool. *Res. Dev.*, **25** (1974), 34-40.
- (12) Davidson, D.L. Fatigue crack plastic zone size and shape through the specimen thickness. *Int. J. Fract.*, **11** (1975), 1047-48.
- (13) Davidson, D.L. The effect of deformation on selected area electron channeling patterns. *J. Mat. Sci. Let.*, **1** (1982), 236-38.
- (14) Joy, D.C. Electron channeling patterns in the SEM. In D.B. Hold, M.D. Muir, P.R. Grant and I.M. Boswarva (Eds.), *Quantitative Scanning Electron Microscopy*. Academic Press, London, New York, San Francisco, 1974. Chapter 5, pp. 131-211.
- (15) Davidson, D.L. Uses of electron channeling in studying material deformation. *International Metals Reviews*, **29** (1984), 75-95.
- (16) Davidson, D.L. **The use of channeling contrast in the study of material deformation.** Proc. of the 10th Annual SEM Symp., 1977, pp. 431-38.
- (17) Gerberich, W.W., J.K. Sheth, and M. Kaczorowski. Fatigue-Induced nanoscale patterns and microstructures. In D. Walgraef (Ed.), *NATO Adv. Workshop on Patterns, Defects and Microstructures in Nonequilibrium Systems*, Austin, TX, March (1986).
- (18) Peterson, K.A. Ph.D. Thesis, Chem. Eng. and Mat. Sci., University of Minnesota, Minneapolis, 1983.
- (19) Stickler, R., C.W. Hughes, and G.R. Booker. Application of the SAACP method to deformation studies. In O. Johari (Ed.), *Scanning Electron Microscopy*, Chicago, IL, Illinois Institute of Technology Research Institute, 1971, pp. 475-480.
- (20) Kaczorowski M., and W.W. Gerberich. The dependence of electron channeling line width degradation on deformation mode. Accepted for publ. in *Scripta Met.* (1986).
- (21) Davidson, D.L. Rotation between SEM micrographs and electron channeling patterns, *J. Phys. E: Sci. Instrum.*, **9** (1976), 341-43.
- (22) Kaczorowski, M. Unpublished results.
- (23) Chin, G.Y., W.L. Mammel, and M.T. Dolan, *Trans. AIME*, **245** (1969), p. 383.
- (24) Gerberich, W.W., A.G. Wright, E. Kruman, and K.A. Peterson. Plasticity contribution to cleavage: Electron channeling and fractographic analysis. In W.W. Gerberich and D.L. Davidson (Eds.), *Fracture: Measurement of Localized Deformation by Novel Techniques*, Conf. Proc., The Met. Soc. AIME, Sept. 1984, pp. 59-74.
- (25) Jago, R.A. and N. Hansen. Grain size effects in the deformation of polycrystalline iron. *Acta Met.*, **34** (1986), 1710-1720.